Published on 12 September 2018. Downloaded by Library of Chinese Academy of Sciences on 5/20/2019 6:59:12 AM.

Nanoscale

ROYAL SOCIETY OF CHEMISTRY

PAPER

View Article Online
View Journal | View Issue

Cite this: *Nanoscale*, 2018, **10**, 18774

Electrically pumped Fabry–Perot microlasers from single Ga-doped ZnO microbelt based heterostructure diodes†

Zhanguo Li,[a,b] Mingming Jiang,*[a,c] Yuzhou Sun,[a,b] Zhenzhong Zhang,[a] Binghui Li,[a] Haifeng Zhao,[a] Chongxin Shan*[a,d] and Dezhen Shen*[a]

Received 10th July 2018,
Accepted 11th September 2018

DOI: 10.1039/c8nr05559a

rsc.li/nanoscale

Semiconducting micro/nanostructures possessing naturally optical waveguiding behaviors and Fabry–Perot (F–P) like resonances are emerging as versatile building blocks for the assembly of photonic and optoelectronic devices, such as photodetectors, light-emitting diodes, lasers and so on. Individual ZnO micro/nanowires with a rectangular cross-section, such as microwires and microbelts possessing naturally smooth facets along both sides for good optical feedback, can be employed as an underlying F–P mode microcavity whilst as the gain medium for light amplification. In this context, electrically pumped F–P mode microlasers comprising a single ZnO:Ga microbelt and p-GaN substrate have been realized. By treating as the precondition, electrically driven exciton–polariton light-emitting behavior was achieved from the heterojunction diodes, which could be ascribed to strong exciton–photon coupling and wave-guided nature of the synthesized microbelts. Once the applied bias exceeded the threshold value, an electrically pumped F–P mode lasing behavior could be observed, the lasing peaks centered at 410.5 nm and 450.5 nm respectively, accompanied with a dramatic narrowing of the spectral line-width to be around 1.0 nm emerging on the waveguided emission spectrum. Therefore, the realization of electrically pumped F–P mode lasing using single microbelt based heterojunction diodes opens the door not only to the fabrication of coherent light sources and model systems for waveguided resonators, but also affords a competitive candidate to develop electrically pumped and ultralow threshold polariton lasers.

1. Introduction

Owing to the natural optical resonant cavities, tunable optoelectronic properties, low-cost, controlled fabrication, *etc.*, semiconducting micro/nanostructures have great potential in the application of micrometer-scale laser sources.[1–9] While plentiful designed architectures for microlasers have been investigated, micro/nanostructures with different microscopic sizes, a high quality factor Q and low lasing threshold excitation power have unleashed their potential as building blocks to construct whispering-gallery mode (WGM) lasers, Fabry–Perot (F–P) mode lasers and random lasers.[10–16] Owing to its direct wide bandgap of 3.37 eV and the large exciton binding energy of 60 meV, ZnO has been employed as a promising material for short-wavelength photoelectronic applications, such as ultraviolet (UV) lasers, photodetectors, and so on.[17–21] By means of relatively simple and inexpensive fabrication methods, such as vapor phase transport, ZnO micro/nanostructures with high crystallinity and smooth boundaries have been synthesized. For example, individual ZnO microwires with a hexagonal cross section, possessing uniform and well-defined geometric structures, have been employed to achieve WGM-mode lasing behavior. Meanwhile, single ZnO nanowires, as well as ZnO microwires with quadrilateral cross section have been used to realize F–P mode lasing characteristics.[17,22–26]

Owing to the difficulty in producing high-quality p-type ZnO, electrically pumped ZnO-based lasers have been reported using heterostructured diodes, such as a ZnO/SiC heterojunction, a ZnO/p-GaN heterojunction, *etc.* Especially, ZnO micro/nanowires with a hexagonal cross section have become attractive candidates to construct electrically pumped heterostructured WGM-mode microlasers under forward bias, as well as

[a] State Key Laboratory of Luminescence and Applications, Changchun Institute of Optics, Fine Mechanics and Physics, Chinese Academy of Sciences, No.3888 Dongnanhu Road, Changchun, 130033, China.
E-mail: mmjiang@nuaa.edu.cn, cxshan@zzu.edu.cn, shendz@ciomp.ac.cn
[b] University of the Chinese Academy of Sciences, Beijing 100049, China
[c] College of Science, Nanjing University of Aeronautics and Astronautics, Nanjing 210016, China
[d] School of Physics and Engineering, Zhengzhou University, Zhengzhou 450001, China

† Electronic supplementary information (ESI) available. See DOI: 10.1039/C8NR05559A

 This journal is © The Royal Society of Chemistry 2018

Published on 12 September 2018. Downloaded by Library of Chinese Academy of Sciences on 5/20/2019 6:59:12 AM.

reverse bias.[10,12,27–31] However, little literature has been reported on the fabrication of electrically pumped F–P mode microlasers. In the case of single ZnO nanowires and microwires with a quadrilateral cross section and microbelts, a natural microcavity is provided for F–P mode lasing with a low lasing threshold, distinct F–P lasing modes, and definite lasing output directions.[15,16,32,33] Thus, it is desirable to fabricate microlasers involving ZnO microstructures and p-GaN to achieve electrically pumped F–P mode lasing characteristics.

In this context, higher crystal quality Ga-doped ZnO (ZnO:Ga) microbelts were synthesized *via* carbothermal reduction methods. Heterostructured light-emitting diodes comprising a single ZnO:Ga microbelt and p-GaN layer were fabricated. Under forward bias, a higher crystal quality and Ga-incorporation were employed to construct more highly efficient light-emitting diodes. With increasing forward currents, the interfacial emissions can be suppressed effectively, and then a typical near-band-emission (NBE) of the ZnO:Ga microbelts dominated the electroluminescence (EL). In particular, when operated under a reverse bias, waveguided output light-emitting behavior can be obtained, which could be attributed to exciton–polariton effects, with the dominant emission wavelengths centered at 407.5 nm. When the reversed bias exceeded the threshold value, electrically pumped lasing behaviors were demonstrated, such as two sharp lasing emission peaks centered at 410.5 nm and 450.5 nm, and a full width at half maximum (FWHM) narrowing to around 1.0 nm was observed in the waveguided output spectrum. Thus, the gain was now large enough to enable the cavity resonance confined in the quasi-rectangular cross section of the ZnO:Ga microbelts. To probe into the electrically pumped lasing characteristics and the exciton–polariton coupling interaction, the resonant process, lasing output modes and quality factor (Q) were investigated theoretically and experimentally. As a consequence, single ZnO:Ga microbelt can be used to construct electrically pumped F–P mode microlasers.

2. Experimental section

ZnO:Ga microbelts have been synthesized *via* a simple one-step chemical vapor deposition (CVD) method in a horizontal dual temperature tube furnace (HF-Kejing: OTF-1500X-II).[34–36] A mixture of high-purity powders with the weight ratio of $ZnO:Ga_2O_3$:graphite (C) = 9 : 1 : 10, which served as the precursors, was placed in a corundum boat. Cleaned Si (100) substrates (without any catalyst coating) were placed on the corundum boat to collect the products. During the synthesis process, a constant flow of argon (Ar) (99.99%) (150 sccm) was introduced into the tube furnace as the carrier gas. Owing to the lower growth temperature of ZnO (950 °C) than that of Ga_2O_3 (1100 °C) in a vapor–solid process, the furnace temperature was firstly increased to 1150 °C in advance; then, the precursor mixtures were placed into the hottest area, leading to intensive mixing of the Ga and Zn vapors. The high-temperature growth environment could make Ga substitute Zn effectively. After maintaining oxygen-free synthesis conditions for 20 min, 8% oxygen (O_2) was introduced into the tube furnaces as the growth gas. The width of the microbelts ranged from 5 to 100 μm, and the length can be up to 1 cm. Meanwhile, to fabricate ZnO:Ga microbelts with higher crystallization quality and controlled surface morphologies, the growth temperature and the reaction times should be increased and extended accordingly.

To investigate the influences of Ga-incorporation on the electrical conductances of the single ZnO:Ga microbelt, the microbelts were selected and transferred onto quartz substrates. Two indium (In) particles were then applied to fix both ends of the microbelts, serving as two electrodes to form a metal–semiconductor–metal (MSM) structure. After annealing for about 5 minutes at 200 °C, the ZnO:Ga microbelts can be fixed on the substrate. In addition, heterostructured light-emitting devices were fabricated as follows: (1) the p-GaN substrate was cleaned; (2) MgO layers were then deposited using molecular beam epitaxy, serving as an insulating layer; (3) the Au and Ni/Au electrodes were deposited on GaN using the electron-beam evaporation system, with the electrode size to be about 0.5 mm in diameter, and; (4) finally, a single ZnO:Ga microbelt was selected and transferred across the boundary between the MgO and GaN films, accompanied with the In particle fixed to the microbelt on the insulating layer serving as the electrode. A schematic diagram of the electrically driven light-emitting device involving a single ZnO:Ga microbelt based heterostructure is shown in Fig. S1.† Therefore, heterostructured light-emitting devices were fabricated.[35]

The surface morphologies of the ZnO:Ga microbelts were characterized using a Hitachi S-3000N/S-4800 scanning electron microscope (SEM), and elemental mapping using energy dispersive X-ray spectroscopy (EDX) was performed. The current–voltage (I–V) characteristics of the devices were measured using a Keithley 2611 system. Photoluminescence (PL) measurements were performed using a He–Cd laser at 325 nm in a LABRAM-UV Jobin Yvon spectrometer. The optically pumped lasing of the ZnO:Ga microbelts was excited using a femtosecond pulsed laser at 325 nm. The EL emissions were collected using a Hitachi F4500 spectrometer. Optical microscope images and EL emissions videos were recorded using an optical microscope.

3. Results and discussion

Fig. 1(a) shows a typical SEM image of the ZnO:Ga microbelts. Fig. 1(b) demonstrates that the synthesized ZnO:Ga microbelts possessed a rectangular cross section. The microbelt has flat and smooth side surfaces, and a rectangular cross-section with the width and thickness around 100 μm and 5 μm, respectively.[16] To characterize the optical properties of the ZnO:Ga microbelts, room temperature PL measurements were carried out using a He–Cd laser with an excitation wavelength of 325 nm. It was demonstrated that the PL spectrum was composed of two main bands: one is a typical NBE excitonic radia-

Published on 12 September 2018. Downloaded by Library of Chinese Academy of Sciences on 5/20/2019 6:59:12 AM.

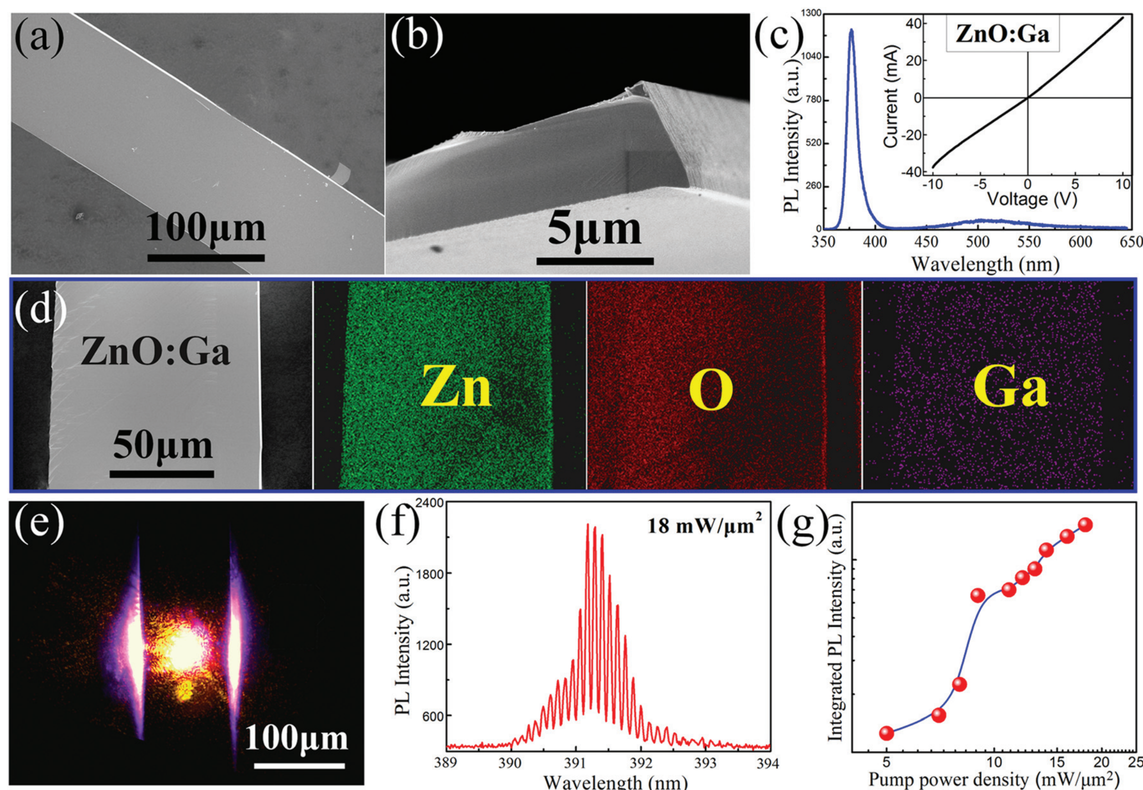

Fig. 1 (a) SEM image of a ZnO:Ga microbelt, possessing a smooth surface. (b) SEM image of a ZnO:Ga microbelt, which possesses a quadrilateral cross section. (c) Room temperature PL emission from single ZnO:Ga microbelts, with the dominant emission wavelength centered at 377.5 nm; the inset demonstrates the *I–V* characteristic of a single ZnO:Ga microbelt. (d) EDX mapping of Zn, O, and Ga elemental distributions. (e) CCD images of the emission from ZnO:Ga microbelts, with the laser pumped at 18 mW μm^{-2}. (f) PL spectrum of the ZnO:Ga microbelt, with optical pumping at 18 mW μm^{-2} power densities. (g) Nonlinear relationship between the integrated emission intensities *versus* the excitation powers. The lasing threshold was extracted to be about 8 mW μm^{-2}.

tive recombination in the UV band, with the dominant emission wavelengths centered at 378 nm; the other is a broad deep donor level related emission in the visible range (Fig. 1(c)). It is clear that the NBE-type emission dominates the PL emission in the UV region. With regard to the undoped ZnO micro/nanostructures, the surface morphology and size of the microbelts is closely related to the surface states and/or surface defects, which may originate from the intrinsic defects, such as zinc interstitials (Zn_i), zinc antisite (Zn_O), and/or oxygen vacancies (V_O).[37–40] As previously reported, Ga-incorporation can lead to lattice expansion due to the substitution of Ga for Zn. Thereby, the origin of the visible emission could be attributed to native defects such as ionized oxygen vacancies, or a Ga_{Zn}-related induced donor impurity level.[40–42] An experimental set-up of a single ZnO:Ga microbelt based MSM structure was built up. The *I–V* curve indicated a linear and symmetric characteristic, which revealed the ohmic contacts between the In electrodes and the ZnO:Ga microbelts, as shown in the inset of Fig. 1(c). Owing to Ga-incorporation, the individual ZnO microbelts can sustain high current densities. In addition, to verify that the enhancement of electrical conductance was dominated by Ga-incorporation, elemental mapping using energy-dispersive X-ray spectroscopy (EDX) was performed to determine the internal structure and composition of the ZnO:Ga microbelts, and the corresponding elemental mappings of Zn, O and Ga are displayed in Fig. 1(d). Within the spatial resolution of the EDX mapping, the distribution of the Ga dopants was uniform throughout the microbelts.[34,41,43] Therefore, these results demonstrate directly that the n-type conductivity in our samples is indeed dominated by Ga-incorporation.[34,38]

To demonstrate that the synthesized ZnO:Ga microbelts possessed a higher crystal quality, an optically pumped lasing measurement was carried out using a confocal microphotoluminescence (μ-PL) spectroscopy system, with a neodymium-doped yttrium aluminum garnet (Nd:YAG) pulse laser (355 nm,10 Hz, 6 ns) employed as the excitation light source. Fig. 1(e) shows an optical image of the photoexcitation with the excitation power being 18 mW μm^{-2}. Clearly displayed are broad symmetrically distributed emission regions, and the light emitted from the lateral sides of the microbelts. Meanwhile, some sharp emission peaks with FWHM $\delta\lambda$ ~0.11 nm emerged from the PL spectra. A lasing action with a mode spacing of $\Delta\lambda$ ~0.12 nm can be distinguished in the emission spectrum. The quality (Q) factor could be calculated to be 3132.5 according to the definition $Q = \lambda/\delta\lambda$, where λ is the

 This journal is © The Royal Society of Chemistry 2018

Published on 12 September 2018. Downloaded by Library of Chinese Academy of Sciences on 5/20/2019 6:59:12 AM.

PL resonant emission wavelength. Fig. 1(g) demonstrates the nonlinear relationship between the input excitation power and the output PL emission intensities, suggesting a transition from spontaneous emission into stimulated emission. It is well-known that mode spacing is the clearest distinction between the F–P type modes and WGM-type modes. According to the equation of the mode spacing for an F–P cavity $\Delta\lambda = \lambda^2/[2L(n - \lambda dn/d\lambda)]$, where L is the cavity length, n = 2.5 is the refractive index of ZnO:Ga, and $dn/d\lambda = -0.015\ nm^{-1}$ at 391.2 nm denotes the dispersion relation for the refractive index, and $\Delta\lambda$ = 0.12 nm as indicated by the PL spectrum. Thus, a cavity length of L = 80 μm was calculated, which agreed well with the experimental value measured from the SEM images (Fig. 1(a)). This indicated that the observed stimulated emission belongs to the F–P lasing mechanism, which is formed in the cavity along the width direction of the cross section.[15,16,33] That is, both the lateral sides of the microbelts could serve as F–P mode cavity mirrors. Actually, this F–P lasing mechanism can also be confirmed with the aid of dark field optical images of the bare ZnO:Ga microbelts (Fig. 1(e)). All the above experimental results demonstrate that individual ZnO:Ga microbelts can function as F–P mode microcavities and support F–P mode lasing characteristics. In addition, compared with the blueshifting of the PL emission, the lasing wavelengths located around 391.5 nm can be attributed to the formation of electron–hole plasma (EHP) in the ZnO:Ga microbelts, because of Ga-incorporation induced filling of the conductance band.[35,44]

Heterostructured light-emitting devices comprising external pressure induced powered ZnO:Ga microbelts and a p-GaN layer were fabricated. Fig. 2(a) shows the *I–V* curve, suggesting typical rectification characteristics with the turn-on voltage being about 3.24 V. By applying a forward bias at room temperature, bright light emission can be seen clearly through the naked eye, as shown in Fig. 2(b). The emitting regions present an interrupted and uneven brightness, with dark regions maybe caused by local poor contact due to uneven pressure exerted between the ZnO:Ga microbelt and GaN layer. Under lower forward injection currents, such as 8.0 mA, the heterostructured diode emitted bright blue-ultraviolet light. On increasing the forward injection currents to 20.0 mA, the heterostructured diode emitted bright ultraviolet light. Once the forward injection currents exceeded 31.0 mA, dazzling ultraviolet light can be observed from the heterostructured diode. Furthermore, the emitted photons were also collected. Under lower injection currents ranging from 3.0 mA to 14.0 mA, the dominant emission wavelengths centered at 420 nm can be derived from the interfacial emissions between the powered ZnO:Ga microbelts and the p-GaN layer, as shown in Fig. 2(c). On increasing the forward injection currents in the range from 16.0 mA to 28.0 mA, bimodal EL emissions could be observed, with the dominant emission wavelengths centered at 376 and 420 nm. Interestingly, increasing the forward injection currents can result in the progressive suppression of the interfacial emissions (420 nm), accompanied with the typical NBE emission of the ZnO:Ga microbelts governing the EL emissions gradually (Fig. 2(d)). Once the forward injection currents exceed 28.0 mA, the emission wavelengths centered at 377.5 nm dominate the EL emission of the diode. Therefore, typical NBE emission of the ZnO:Ga microbelts dominating the EL emission of the heterostructured diode completely can be realized, accompanied with effective suppression of the interfacial emissions centered at 420 nm, as shown in Fig. 2(e).[35]

In particular, when operated under a reversed bias, the n-type region of the diode would be connected to a higher potential than the p-type region, which resulted in wider depletion region and large built-in electric field across the interfacial junction regions. Then, electrically driven light-emitting characteristics of the heterostructured diode under reverse bias were also investigated.[27,45] Fig. 2(f) revealed the EL emission spectra under lower reversed injection currents ranging from 5.0 to 8.5 mA. The dominant emission wavelengths were centered at 398.5 nm, accompanied with negligible visible emissions. Once the reversed injection currents exceeded a certain value, such as 10.0 mA, a sharp emission peak emerged in the spontaneous emission spectra, with the FWHM narrowing to be around ∼1.0 nm (Fig. 2(g)). To investigate the EL emission characteristics, the integrated EL emission intensities *versus* the reversed injection currents were also measured, as shown in Fig. 2(h). It was revealed that the emission intensities increased as a nonlinear relationship with the reversed injection currents, suggesting the transition from spontaneous emission to stimulated emission. In addition, the narrowing of the FWHM indicated that the spontaneous emission was amplified by the process of stimulated emission in the powered ZnO:Ga microbelts.[27–30] Thus, an electrically driven lasing action was produced from the powered ZnO:Ga microbelt based heterostructured diode under a reversed bias. The emission intensities increased slowly when the injection currents were below 15.0 mA, and then increased relatively rapidly when the current was larger than 15.0 mA. This indicated that the lasing threshold current was estimated to be about 15.0 mA.[17]

To investigate the electrically driven light-emitting mechanism from the single ZnO:Ga microbelt based heterostructured diodes, the energy band diagram of the n-ZnO:Ga/p-GaN heterostructures was studied. Firstly, at lower forward injection currents, the EL spectra displayed that the dominant emission wavelengths centered at 420 nm could be attributed to interfacial emissions, which formed at the ZnO:Ga/GaN heterostructural interface (Fig. 2(c)). Meanwhile, the FWHM narrowed to be about 45 nm, which was much wider than that in the PL spectrum from a single ZnO:Ga microbelt (Fig. 1(c)). Thus, an energy barrier was formed towards the ZnO:Ga/GaN heterostructural interface, which is likely to be determined by the fabrication process, and the barriers at the interface for the holes and the electrons are approximately equal. Thereby, the emissions from ZnO:Ga, p-GaN and the interface together contributed to the EL emissions.[12,46–49] By contrast, PL emission from the ZnO:Ga microbelt (377.5 nm) was derived from typical NBE recombination, while the emission centered at

Published on 12 September 2018. Downloaded by Library of Chinese Academy of Sciences on 5/20/2019 6:59:12 AM.

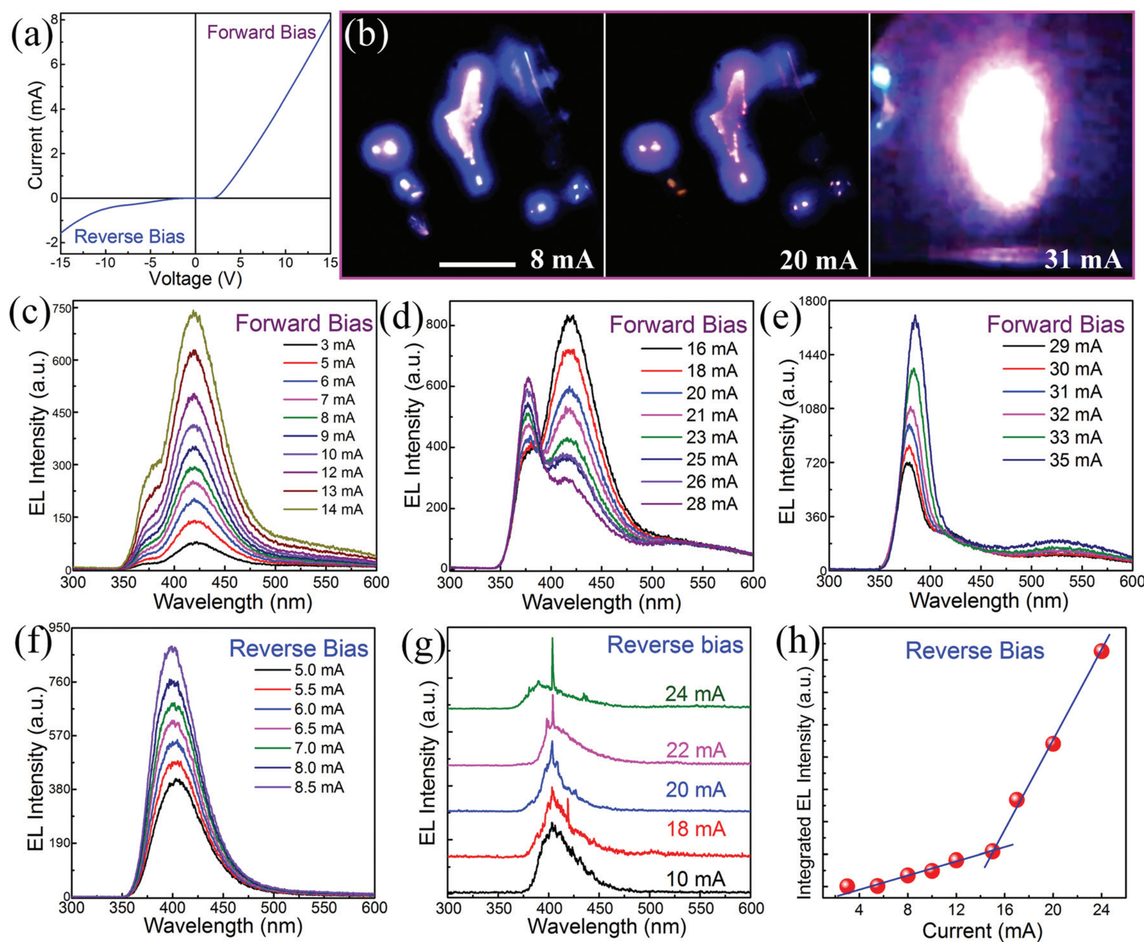

Fig. 2 (a) *I–V* characteristic of heterojunction diodes comprising a single ZnO:Ga microbelt and p-GaN layer. (b) Micrographs of bright blue-ultraviolet light emission from the heterojunction diode at room-temperature, with the forward injection currents ranging from 8.0 mA to 31.0 mA. (c) EL emission spectra of the single ZnO:Ga microbelt based heterojunction diode under the forward injection currents ranging from 3.0 mA to 14.0 mA, with the dominant emission wavelengths centered at 420 nm. (d) On increasing the injection currents, the EL emissions can be transferred from interfacial emission (420 nm) to the typical NBE of the ZnO:Ga microbelt (383.4 nm). (e) EL emission spectra of the heterojunction diode when the forward injection currents ranged from 29.0 mA to 35.0 mA, with the dominant emission wavelengths centered at 384.5 nm. When operated at reversed bias, (f) the EL emission spectra demonstrated the dominant emission wavelengths centered at 398.2 nm with injection currents ranging from 5.0 mA to 8.5 mA; (g) once the injection currents exceeded 10.0 mA, a sharp emission peak with FWHM narrowing to be ~1.0 nm appeared in the spectra, with the dominant emission wavelengths redshifted to 402.5 nm; (h) nonlinear relationship between the integrated EL emission intensities *via* the reversed currents.

450 nm can be derived from Mg-related deep acceptor levels in p-GaN. Thus, the emission centered at 420 nm can be attributed to interfacial radiative recombination of the electrons from n-ZnO:Ga, accompanied with holes originating from p-GaN. The barrier heights towards the interface for the holes and the electrons was calculated to be 0.42 eV and 0.44 eV, respectively. The energy band diagram is displayed at zero bias in Fig. 3(a). Under lower forward injection currents, the wide EL emission band is attributed to the superposition of a strong ZnO:Ga near bandgap recombination, a relatively strong interface radiation, and a much weaker emission from p-GaN. With increasing forward injection currents, the governed EL emissions turned into the typical NBE emissions of ZnO:Ga, accompanied with efficient suppression of the interfacial emissions. Under larger forward injection currents, the energy band diagram of the n-ZnO:Ga/p-GaN heterojunction can be depicted as shown in Fig. 3(b).

Under reverse bias, the energy band diagram of the n-ZnO:Ga/p-GaN heterostructures was also characterized, and is illustrated in Fig. 3(c). Owing to the electrical potential difference between the electron affinity energies and the bandgap E_g of ZnO:Ga and GaN, the energy barrier for the electrons $\Delta E_C = \chi_{ZnO} - \chi_{GaN}$ is higher than that for the holes ($\Delta E_V = E_{g(ZnO)} + \chi_{ZnO} - E_{g(GaN)} - \chi_{GaN}$) near the interface between the n-ZnO:Ga microbelt and the p-GaN layer.[10,46,50] At lower reversed bias, holes could be injected into the unoccupied valence band minimum of ZnO:Ga, while electrons were being injected into the occupied valence band maximum of p-GaN. Thus, the unoccupied states of the conduction band of n-ZnO:Ga would be lower than the occupied states of the valence band of

Published on 12 September 2018. Downloaded by Library of Chinese Academy of Sciences on 5/20/2019 6:59:12 AM.

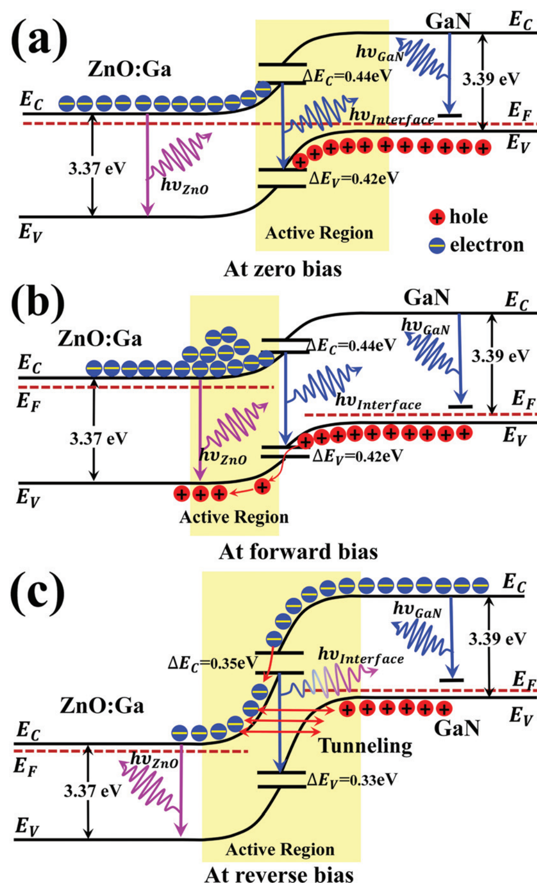

Fig. 3 Band diagram of the n-ZnO:Ga microbelts/p-GaN heterostructured light-emitting devices: (a) at zero bias, (b) at forward bias, and (c) at reverse bias.

p-GaN. Then, the electrons would be more inclined to move toward lower energy, rather than radiatively recombining with Mg-related deep acceptor levels in the valence band. Once the applied reversed bias reached a breakdown, radiative recombination was considered to be occurring in the interfacial contact regions of the heterostructures. By means of Gaussian fitting, the broad EL spectra could be deconvoluted into three distinct subbands, which were centered at 375 nm, 408 nm and 450 nm, as shown in Fig. S2.† The UV emission band centered at 375 nm can be attributed to the NBE-type emission of the ZnO:Ga microbelts, while the blue emission band centered at about 450 nm could be ascribed to transitions from the conduction band or unidentified shallow donors to Mg-related deep acceptor levels in the p-GaN layer. The emission band centered at around 408 nm can be attributed to interfacial radiative recombination of the electrons from the ZnO:Ga microbelts and holes from the Mg-related deep acceptor levels of p-GaN. Considering the EL spectra, which were dominated by a violet emission centered at 400 nm with a FWHM of ∼40 nm, EL emissions can be derived from irradiative electron–hole recombination in the ZnO:Ga microbelts, as well as interfacial emission. To further increase the reversed injection currents, the overall band structure of p-GaN shifted upward, which could result in bending of the heterojunctional barrier. The barrier band would be more inclined, which can even make the maximum valance band of p-GaN higher than the minimum conduction band of ZnO:Ga. This will cause the thickness of the tunneling barrier to be closer to the broken-gap band at the p–n junction. Furthermore, a high strength built-in electrical field can be formed across the heterojunction, and this electrical field will enable the electrons of the valance band to obtain additional potential energy. Thus, the electrons could tunnel across the narrow barrier from the valence band of p-GaN to the conduction band of ZnO:Ga and get captured by the Mg-related deep acceptor level near the interface, yielding interfacial emission. In addition, large amounts of electrons would be pulled into ZnO:Ga through the conduction band of p-GaN by this large reverse electric field. As these electrons drift across the interface between GaN and ZnO:Ga, some of them recombine with holes in the Mg-related deep levels and interface states to produce interfacial emission. The rest of these electrons arrive at the conduction band of ZnO:Ga and recombine with the holes in the valance band of ZnO:Ga to generate NBE-type emission.

It was further exhibited that the synthesized ZnO:Ga microbelts possessed high crystallinity and smooth boundaries, and could be employed as an excellent natural resonance microcavity to construct electrically pumped F–P mode ultraviolet lasers. A single ZnO:Ga microbelt was selected to construct a heterostructured diode, with the schematic diagram shown in Fig. 4(a). Fig. 4(b) demonstrates the experimental set-up used to explore light-emission from an electrically driven single ZnO:Ga microbelt based heterostructured diode at room temperature. The *I–V* curve shown in Fig. 4(c) indicates typical rectifying behavior between the ZnO:Ga microbelt and p-GaN layer, resulting in the formation of a p–n heterojunction, with the forward turn on voltage estimated to be about 3.35 V. It is considered that the linear *I–V* curve revealed good ohmic contact between the In electrodes and the ZnO:Ga microbelt, while Ni/Au also formed good ohmic contact with p-GaN, as reported before.[35] Therefore, the diode-like rectification can be derived from the n-ZnO:Ga microbelt and p-GaN heterostructure. Under forward bias, electrically driven light-emission from a single ZnO:Ga microbelt based heterojunction diodes was carried out, and the emission characteristics can be referred to in Fig. S3.†[35] When operated under reversed bias, blue purple lighting can be observed from the heterojunction diodes, and the brightness and light-emitting regions increase with the driven currents. A typical optical microscope image of the EL emission from the heterostructured devices was also collected, with the emission regions distributed along both lateral sides of the microbelt, as shown in Fig. 4(d). The bright emission regions indicated that EL emissions could be derived from the heterostructured junction, where electrons from the ZnO:Ga microbelts radiatively recombined with the holes originated from p-GaN. Compared with the lighting behavior from electri-

View Article Online

Published on 12 September 2018. Downloaded by Library of Chinese Academy of Sciences on 5/20/2019 6:59:12 AM.

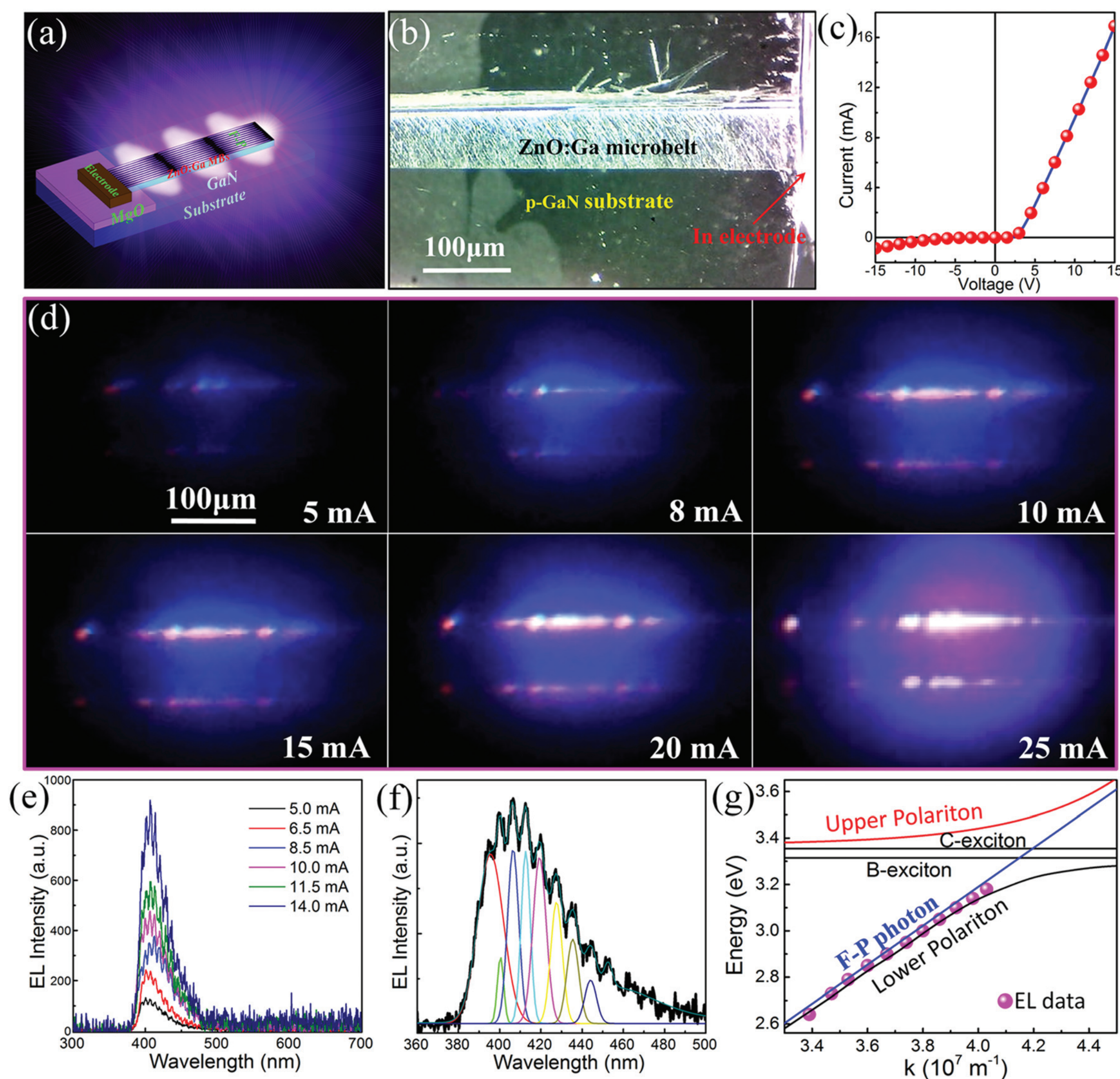

Fig. 4 (a) Schematic diagram of the heterostructured diodes, utilizing ZnO:Ga microbelts as the gain medium, and a p-GaN layer being treated as the holes injection layer, with electrically driven light-emission observed from both sides of the microbelts. (b) Micrograph of the heterostructured light-emitting devices comprising a single ZnO:Ga microbelt and p-GaN substrate. (c) *I–V* characteristic illustrated rectifying characteristic between the ZnO:Ga microbelt and p-GaN layer, suggesting the formation of a p–n junction. (d) Micrographs of the bright blue-ultraviolet light-emission from the heterojunction diode operated under reversed injection currents, with the light-emitting regions localized towards both facets of the microbelt. (e) EL emission spectra of the single ZnO:Ga microbelt based heterojunction diode with reversed injection currents rangeing from 5.0 mA to 14.0 mA, the dominant emission wavelengths centered at 407.5 nm. (f) EL emission spectrum acquired from the heterojunction diode, displaying multiple F–P interference peaks that were fitted with Lorentzian line shapes to determine the separate resonance energies completely. (g) Corresponding energy-wave vector dispersion curves confined in the rectangular cross section: the energies of the B-exciton and C-exciton denoted as black solid lines, and the dispersion of the pure F–P photon denoted with blue lines were also described, with parameters that could be referred to in literature reports;[47,51,52] red and black solid lines represent the upper and lower branches of the polariton; and the purple solid spheres are the experimental data extracted from (f).

cally driven light-emission from powered ZnO:Ga microbelt based heterostructured diodes, the distribution of the emission regions can be ascribed to the F–P mode optical microcavities, which formed between both sides of the microbelt.

Fig. 4(e) displays the EL spectra of the heterostructured diode at room temperature, with reversed injection currents ranging from 5.0 mA to 14.0 mA. A strong UV emission and a negligible visible emission were observed, with the dominant emission wavelengths centered at 407.5 nm. Besides, it was noted that a series of interfering emission peaks were well resolved from the EL emission spectra, indicating waveguided behaviors.[47,53] This can be ascribed to the F–P mode optical microcavities which were formed by the smooth rectangular cross section of the microbelts. For the F–P like cavities, the rectangular structure played an important role in producing a

 This journal is © The Royal Society of Chemistry 2018

View Article Online

Published on 12 September 2018. Downloaded by Library of Chinese Academy of Sciences on 5/20/2019 6:59:12 AM.

waveguided output. Thus, the planes of the opposite side of the single ZnO:Ga microbelts could be used to construct F–P mode optical microcavities, with the bilateral facets serving as the F–P mirrors. Next, we studied the underlying mechanism of the EL emission spectra, as shown in Fig. 4(f). One can see that the energy spacing between the neighboring modes are becoming smaller with the energy shifting towards the exciton resonance. This phenomenon could be attributed to the classical F–P resonances. Since the energies of the optical modes in the ultraviolet region are close to those of the excitons, a strong interaction between these modes and the excitons was expected, and the exciton–polariton effect should be included for a proper understanding of the ultraviolet EL emission spectra of ZnO:Ga microbelts.[47,51,52,54] The series of peaks can be attributed to the excition–polariton effect from the strong coupling between the cavity modes (with different mode numbers) and the excitons of the ZnO:Ga gain medium. For the EL spectra shown in Fig. 4(f), considering that there is a reflective facet in the microbelts which can form F–P optical cavities, the cavity length L can be calculated by the formula: $\delta\lambda \approx \lambda^2/2nL$, where n is the refractive index (n = 2.5 for ZnO:Ga), λ is the resonant wavelength, and $\delta\lambda$ is the mode spacing. The calculated cavity length is about 5 μm, which is much shorter than the measured width of the synthesized ZnO:Ga microbelts, but very close to the thickness of the ZnO:Ga microbelts. Thus, it can be concluded that photon oscillation was confined within the upper and lower surfaces. From the waveguided spectra and optical microscopic images, it could be deduced that the upper and lower surfaces of the microbelts could not serve as optical resonant cavity mirrors, and it is more apt to be employed to support the waveguided channel for the generated photons. Therefore, a single ZnO:Ga microbelt with a rectangular cross section can function as a well-defined waveguide.

Compared with macroscopic crystals, light–matter interaction is much stronger when confined in semiconducting nanostructures. For example, exciton–polariton behaviors have been used to govern the properties of ZnO micro/nanocavities, such as nanowires and microwires with a hexagonal cross section. Being treated as photon-like behavior, the exciton–polariton dispersion relation can be expressed as following:[47,51,54,55]

$$E(\omega,\vec{k}) = \hbar\omega(\vec{k}) = \frac{\hbar c\vec{k}}{\sqrt{\varepsilon_\mathrm{b}\left(1+\frac{{\omega_\mathrm{L}}^2-{\omega_\mathrm{T}}^2}{{\omega_\mathrm{T}}^2-\omega^2-i\omega\gamma}\right)}} \tag{1}$$

where ε_b is the background dielectric constant, and ω_L and ω_T are the longitudinal and transverse resonance frequencies of the excitons, respectively. Thus, eqn (1) provides the energy levels of the upper and lower branches of a propagating exciton–polariton, as a function of its wave vector $\vec{k}$. The polariton effects in the ZnO:Ga microbelts can be well described by the coupling oscillator model. The refractive index and polariton dispersion can be described using the simple dielectric approximation form as follows:

$$\begin{aligned} n^2 = \varepsilon(\omega,k) &= \varepsilon_\mathrm{b}\left(1+\sum_{i=A,B,C}\Omega_i\frac{{\omega_{i,\mathrm{L}}}^2-{\omega_{i,\mathrm{T}}}^2}{{\omega_{i,\mathrm{T}}}^2-\omega^2-i\omega\Gamma_i}\right) \\ &= \frac{c^2k^2}{\omega^2} \end{aligned} \tag{2}$$

where n is the refractive index, ε_b is the background dielectric constant, $\omega_{i,\mathrm{T}}$ and $\omega_{i,\mathrm{L}}$ are the transverse and longitudinal resonance frequencies, and Γ_i is the damping constant.[47,51,53,55] Owing to eqn (2), the dispersion relationship curves can be separated into an upper exciton–polariton branch and a lower exciton–polariton branch, with the energy gap between these two branches being approximately identified as Rabi splitting. On combination with Fig. 4(f), energy-wavevector dispersion curves could be depicted, as shown in Fig. 4(g). The upper branch (red solid line) and lower branch (black solid line) have been marked with two colors. The generated photons and excitons energy dispersion relation, which were confined in the quasi-rectangular cross section were also demonstrated, and denoted as a blue solid line. To probe into the exciton–polariton dispersion, the peaks were extracted from the EL emission spectrum (Fig. 4(f)). The Rabi splitting between the polariton branches is as high as 250 meV. It can be confirmed that the experimental results were well coincident with the exciton–polariton dispersion curves, which was derived from the strong coupling between the optical F–P modes and excitons. Besides, the result also guaranteed that the EL emissions could be attributed to polariton effects in the ZnO:Ga microbelts when electrically driven.[47,54]

In particular, once the reversed injection currents exceeded a certain value, such as 26.0 mA, two very sharp and separate emission peaks superimposed on the broad spectrum were observed (Fig. 5(a)). The emission peaks were centered at 410.5 nm ($I_{h\nu_1}$) and 450.5 nm ($I_{h\nu_2}$), with a FWHM of ~1.0 nm also detected.[12,27,29,30] Fig. 5(b) displays the EL emission intensities with increasing reversed injection currents. With an increase of the reversed injection currents, such as 18.0 mA, a sharp peak centered at 451.5 nm firstly appeared in the emission spectra. On further increasing the injection currents, such as 21.0 mA, other sharp emission peaks could also be observed, indicating conversion of the EL emission behavior. Meanwhile, the emission ratios denoted as $I_{h\nu_2}/I_{h\nu_1}$ could be tuned and depended on an increase of the reversed injection currents, which are shown in the inset of Fig. 5(b). The emission ratios $I_{h\nu_2}/I_{h\nu_1}$ increased gradually, which could be attributed to a strong lasing competition action. Thus, a stable dual-wavelength laser output with different intensities can be achieved through controlling the reversed injection currents. In addition, the gap distance of ~40.0 nm of the two lasing peaks is in close proximity to the bandwidth of the spontaneous emission. The narrowest spectral linewidth of both the peaks was around 1.0 nm, and are significantly broader than the typical spectral linewidth of the optically pumped lasing spectra. The discrepancies could be most likely due to

Published on 12 September 2018. Downloaded by Library of Chinese Academy of Sciences on 5/20/2019 6:59:12 AM.

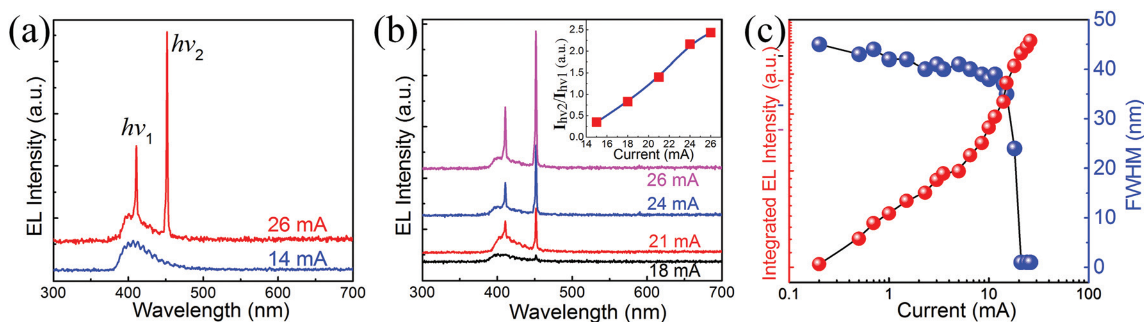

Fig. 5 (a) When the reverse currents exceeded 15.0 mA, such as when 20.0 mA was applied, two sharp emission peaks appeared in the emission spectrum, with the dominant emission wavelengths centered at 410.5 nm ($h\nu_1$) and 451.5 nm ($h\nu_2$) respectively; meanwhile, the FWHM narrowed to around 1.0 nm. (b) The EL emission spectra of the single ZnO:Ga microbelt based heterojunction diode were collected with increasing reversed injection currents from 18.0 mA to 26.0 mA, with the emission peaks ratio $I_{h\nu_2}/I_{h\nu_1}$ dependent on the injection currents displayed in the inset. (c) Integrated EL emission intensities of the heterojunction diodes as a function of the reversed injection currents, and the FWHM as a function of the reversed injection currents, with drastic narrowing of the line width occuring near the threshold current of 18.0 mA.

the following reasons, such as the synthesized ZnO:Ga microbelts possessing an irregularly shaped rectangular cross section (Fig. 4(b)), limitation in the spectrometer resolution, as well as the fabrication of the heterostructured diodes. To further illustrate the lasing characteristics, a relationship in the form of a log–log scale between the integrated emission intensities and the injection currents was depicted, as demonstrated in Fig. 5(c). A typical nonlinear behavior of an "*S*" shape relationship exhibited a transition from a sublinear regime to a superlinear regime. Thus, a reversed injection threshold current of 18.0 mA could be estimated. When the applied reversed current exceeded this current, the emission intensities increased nonlinearly, indicating a transition from spontaneous radiation to stimulated radiation. The spectral linewidth relying on the reversed injection currents was also measured. It displayed that an abrupt decrease emerged, and became narrower from 45.0 nm to 1.0 nm as the reversed injection currents changed from 9.0 mA to 18.0 mA (Fig. 5(c)). Therefore, an electrically driven lasing action was achieved using single ZnO:Ga microbelt based heterojunction diodes.

To further explore the electrically pumped lasing characteristics, a comparison of the normalized F–P mode lasing behavior and the waveguided exciton–polariton lighting was implemented, as displayed in Fig. 6(a). As mentioned above, the waveguided EL emissions can be attributed to strong coupling between the excitons and the generated photons confined in the quasi-rectangular cross section of the ZnO:Ga microbelts. That is, the confined photons can propagate along the cross section direction and oscillate between both the lateral side-facets of the microbelts. In addition, detailed information on the device structures can be referred to in Fig. S4.† The microbelts demonstrated an asymmetric cross-section (Fig. S4(c)†). Thus, a possible EL emission mechanism under reverse bias was studied and is illustrated in Fig. 6(b). The green solid lines were defined as the interfacial surfaces between ZnO:Ga and air, acting as mirrors of the microbelts and providing feedback of the lighting oscillation. Under reversed bias, holes can be injected into the n-ZnO:Ga microbelts, as well as the injection of electron into the p-GaN layers. When the applied reversed bias reached the breakdown, the injected electrons could tunnel through the p-GaN substrate and upwards into the ZnO:Ga microbelts due to the thickness of the p-GaN layer (~200 nm) and lower carrier concentration. Thus, radiative recombination could occur between the interfacial regions, with lighting that can observed from both side-facets of the microbelts. As we mentioned before, the non-homogeneity of the light-emitting regions distribution along both facets of the microbelts may be caused by non-uniform physical contact during the fabrication, as well as the non-uniform distribution of recombination centers (Fig. 4(e)). Meanwhile, the diverse EL emissions under reversed bias could be divided into several sub-bands: (i) the sharp ultraviolet emission centered at 375 nm, which can be ascribed to NBE-type emission from the ZnO:Ga microbelts, (ii) the emission centered around 410 nm, which can be contributed to from the interfacial emissions with the electrons from the conduction band of the ZnO:Ga microbelts and holes from Mg-related deep acceptor levels, (iii) and the emission band around 442 nm, which is likely to be related to Mg-related deep acceptors levels. To investigate the generation mechanism of the two discrete lasing peaks with about 40 nm gap distance, the competition dynamic procedure of the dual-peak lasing, which depends on the optical gain and microcavity loss, was taken into account. During the lighting oscillation, this type of trapezoid cross section may be conducive to achieve the lighting resonant mode competition and selection, such as the end-facet reflection loss, the optical propagation loss, and the material optical gain, which play crucial roles in producing lasing.[56] Owing to the heterojunction diode, the lasing centered at 410.5 nm is related to the NBE-type emission from the ZnO:Ga microbelt. Meanwhile, under high reverse bias, the bandgap near the depletion layer will appear to be bending and become narrower than the bandgap of ZnO:Ga, thus, the lasing peak centered at 450.5 nm would be generated by interfacial recombination (located in the depletion region of the ZnO:Ga microbelt). Thereby, dual independent lasing modes that occurred in the ultraviolet and visible bands affirmed that there

 This journal is © The Royal Society of Chemistry 2018

Published on 12 September 2018. Downloaded by Library of Chinese Academy of Sciences on 5/20/2019 6:59:12 AM.

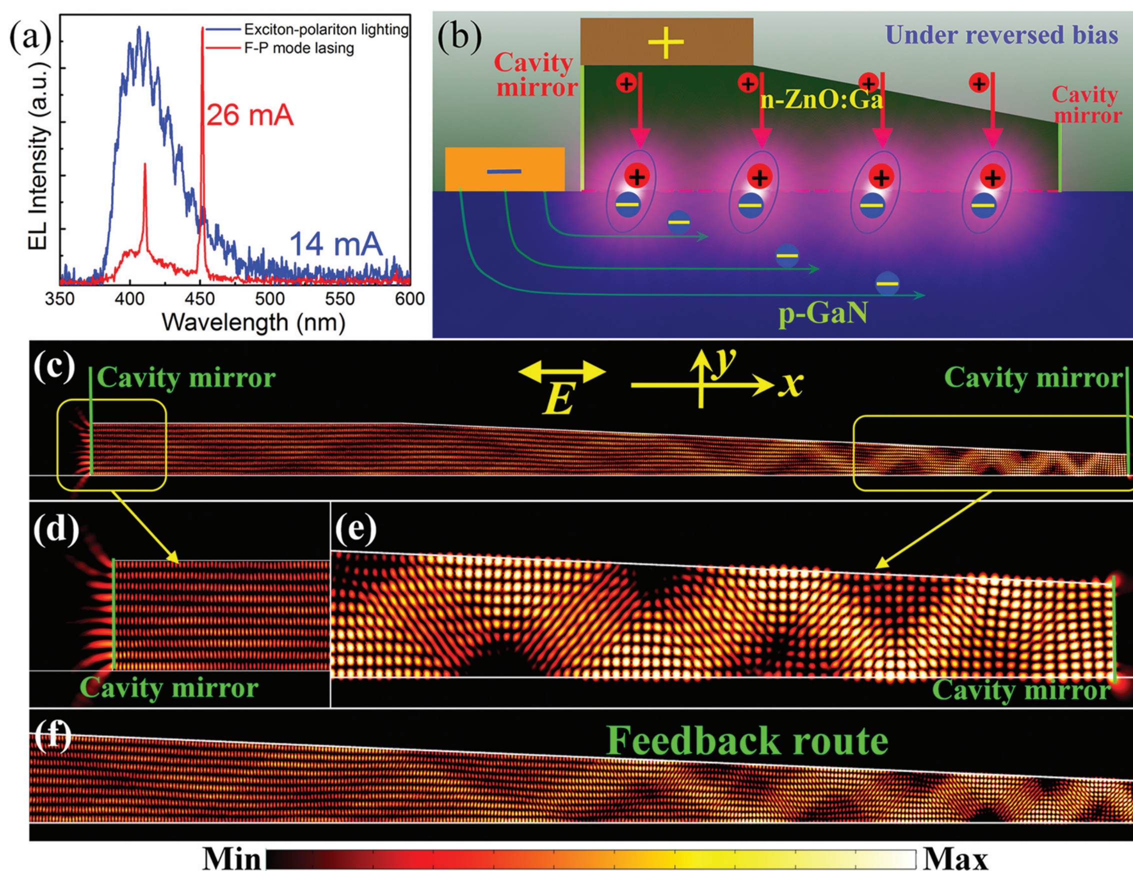

Fig. 6 (a) Comparison of the normalized electrically pumped lasing spectrum, and EL spectrum in the form of F–P waveguided emissions. (b) Schematic illustration of the electrically driven light-emitting dynamic process under reversed bias, the excition (electron–hole pair) recombination mainly occurs at the n-ZnO:Ga/p-GaN heterostructured interface, with the peak centered at 410.5 nm, and the other peak centered at 451.5 nm. (c)–(f) Numerical calculation and simulation on the F–P mode lasing behaviors from a single ZnO:Ga microbelt were carried out, with the standing wave field distributions $E(x,y)$ confined in the rectangular cross section along the x–y plane, with the green solid lines denoted as the cavity mirrors. It is considered that the electron concentration in the ZnO:Ga microbelts is $n \sim 10^{20}$ cm^{-3}, $n_{ZnO} = 2.5$, $n_{quartz} = 1.5$, $n_{air} = 1$, and the sizes of the ZnO:Ga microbelts can be referred to in Fig. S6,† with the corresponding calculated wavelength $\lambda_0 = 410.5$ nm. The center of the microbelts defined the origin ($x = y = 0$).

are two lasing gain regions, which could result in F–P mode resonances confined in the heterostructured diode. Therefore, the lasing peaks in the ultraviolet and visible regions should be attributed to the light emitted from these two regions.

To confirm that the synthesized ZnO:Ga microbelts can be used to construct F–P mode lasing, theoretical calculations and numerical simulations were also carried out. By contrast, a microbelt with a perfect rectangular cross section was also simulated theoretically, as shown in Fig. S5.† In the case of the synthesized ZnO:Ga microbelts (Fig. S4†), a belt with an irregular rectangular cross section was constructed, as shown in Fig. S6.† According to the experimental measurement results, suitable parameters, such as electron concentration $n \sim 10^{21}$ cm^{-3}, have been taken into account as a key consideration. The incident wavelengths were defined as $\lambda_1 = 410.5$ nm, and $\lambda_2 = 450.5$ nm, and other parameters of the modeling can be referred to in Fig. S6.† Standing-wave field resonant modes distributed in the rectangular cross section were numerically simulated with the aid of eigenfrequency analyses of the two-dimensional (2D) time domain and frequency domain finite element method (FDTD).[16,19,35] During the simulation, the incident photons absorption of the cavities was neglected. Standing-wave field distribution $\mathbf{E(x,y)}$ patterns of F–P modes confined in the rectangular cross section are displayed in Fig. 6(c)–(f). It is quite clear that a standing-wave field distribution can be formed between both bilateral sides of the belt. On account of the simulated electric field distribution, the incident photons can propagate back and forth between the lateral sides of the microbelts. Thus, perfect standing wave field distributions were formed. Therefore, ZnO microbelts with a quasi-rectangular cross section can be employed to construct F–P mode lasers.

4. Conclusion

In summary, heterostructured light-emitting devices comprising single a ZnO:Ga microbelt and a p-GaN layer were fabri-

Published on 12 September 2018. Downloaded by Library of Chinese Academy of Sciences on 5/20/2019 6:59:12 AM.

cated to construct F–P mode lasing diodes. An electrically driven exciton–polariton light-emitting behavior can be observed, with the dominant emission wavelengths centered at 407.5 nm when operated at lower reversed bias. The waveguided emission characteristics can be attributed to strong exciton–photon coupling, which happened along the quasi-rectangular cross section of the ZnO:Ga microbelts. The Rabi splitting between the polariton branches is as high as 250 meV. Thus, waveguided output characteristics could be treated as the precondition to construct electrically pumped F–P mode microlasers. In particular, once the reversed bias reached a threshold value, two discrete and sharp lasing peaks centered at 410.5 nm and 450.5 nm, accompanied with the FWHM narrowing to ~1.0 nm, appeared on the emission spectra. The consistent overlap between the F–P mode waveguided emission peaks and the lasing peaks indicated that F–P mode lasing was realized using single ZnO:Ga microbelt based heterojunction diodes. The suppression of some lasing modes could be ascribed to the mode competition over the special photon travelling routes, which confined inside the quasi-trapezoidal cross section of the microbelts. This study illustrated that semiconductor microstructures with rectangular cross sections have the potential to be applied in the fabrication of F–P mode microlasers, as well as electrically pumped polariton lasers.

Conflicts of interest

There are no conflicts to declare.

Acknowledgements

This work was supported by the National Natural Science Foundation of China (Grant No. 11574307 and U1604263), the National Science Fund for Distinguished Young Scholars (Grant No. 11727902, 61425021 and 61525404), and the 100 Talents Program of the Chinese Academy of Sciences.

References

1 X. Wu, Q. Chen, P. Xu, Y. C. Chen, B. Wu, R. M. Coleman, L. Tong and X. Fan, *Nanoscale*, 2018, **10**, 9729–9735.
2 S. W. Eaton, A. Fu, A. B. Wong, C.-Z. Ning and P. Yang, *Nat. Rev. Mater.*, 2016, 16028.
3 Y. Su, C. Liu, S. Brittman, J. Y. Tang, A. Fu, N. Kornienko, Q. Kong and P. Y. Yang, *Nat. Nanotechnol.*, 2016, **11**, 609–612.
4 Q. Deng, M. Kang, D. Zheng, S. Zhang and H. Xu, *Nanoscale*, 2018, **10**, 7431–7439.
5 Y. Huang, Y. Fang, Z. Zhang, L. Zhu and M. Sun, *Light: Sci. Appl.*, 2014, **3**, e199.
6 Y. H. Chou, K. B. Hong, C. T. Chang, T. C. Chang, Z. T. Huang, P. J. Cheng, J. H. Yang, M. H. Lin, T. R. Lin and K. P. Chen, *Nano Lett.*, 2018, **18**, 747–753.
7 G. Beane, B. S. Brown, P. Johns, T. Devkota and G. V. Hartland, *J. Phys. Chem. Lett.*, 2018, **9**, 1676–1681.
8 C. Z. Ning, L. Dou and P. Yang, *Nat. Rev. Mater.*, 2017, **2**, 17070.
9 R. F. Oulton, V. J. Sorger, T. Zentgraf, R. M. Ma, C. Gladden, L. Dai, G. Bartal and X. Zhang, *Nature*, 2009, **461**, 629–632.
10 X. Yang, C. X. Shan, P. N. Ni, M. M. Jiang, A. Chen, H. Zhu, J. H. Zang, Y. J. Lu and D. Shen, *Nanoscale*, 2018, **10**, 9602–9607.
11 C. Xu, J. Dai, G. Zhu, G. Zhu, Y. Lin, J. Li and Z. Shi, *Laser Photonics Rev.*, 2014, **8**, 469–494.
12 J. Dai, C. X. Xu and X. W. Sun, *Adv. Mater.*, 2011, **23**, 4115–4119.
13 X. Duan, Y. Huang, R. Agarwal and C. M. Lieber, *Nature*, 2003, **421**, 241.
14 Z. Zhou, B. Yin and J. Michel, *Light: Sci. Appl.*, 2015, **4**, e358.
15 M. Ding, D. Zhao, B. Yao, Z. Guo, L. Zhang and D. Shen, *Opt. Express*, 2012, **20**, 13657–13662.
16 J. Li, M. Jiang, C. Xu, Y. Wang, Y. Lin, J. Lu and Z. Shi, *Sci. Rep.*, 2015, **5**, 9263.
17 Q. Wang, Y. Yan, F. Qin, C. Xu, X. Liu, P. Tan, N. Shi, S. Hu, L. Li and Y. Zeng, *NPG Asia Mater.*, 2017, **9**, e442.
18 C. Soci, A. Zhang, B. Xiang, S. A. Dayeh, D. P. R. Aplin, J. Park, X. Y. Bao, Y. H. Lo and D. Wang, *Nano Lett.*, 2007, **7**, 1003.
19 S. Chu, G. Wang, W. Zhou, Y. Lin, L. Chernyak, J. Zhao, J. Kong, L. Li, J. Ren and J. Liu, *Nat. Nanotechnol.*, 2011, **6**, 506–510.
20 K. Ding and C. Ning, *Light: Sci. Appl.*, 2012, **1**, e20.
21 H. Kind, H. Yan, B. Messer, M. Law and P. Yang, *Adv. Mater.*, 2010, **14**, 158–160.
22 R. Chen, B. Ling, X. W. Sun and H. D. Sun, *Adv. Mater.*, 2011, **23**, 2199–2204.
23 D. J. Gargas, M. C. Moore, A. Ni, S. W. Chang, Z. Zhang, S. L. Chuang and P. Yang, *ACS Nano*, 2010, **4**, 3270–3276.
24 M. A. Versteegh, D. Vanmaekelbergh and J. I. Dijkhuis, *Phys. Rev. Lett.*, 2012, **108**, 157402.
25 Y. Lai, Y. Lan and T. Lu, *Light: Sci. Appl.*, 2013, **2**, e76.
26 N. Zhang, K. Yu, Q. Li, C. Song, L. Zhu and Z. Zhu, *Mater. Lett.*, 2014, **121**, 231–233.
27 Y. Xu, Y. Li, L. Shi, D. Li, H. Zhang, L. Jin, L. Xu, X. Ma, Y. Zou and J. Yin, *Nanoscale*, 2018, **10**, 5302–5308.
28 G. Zhen, D. Zhao, Y. Liu, D. Shen, B. Yao, Z. Zhang, B. Li, G. Zhen and Y. Liu, *J. Phys. Chem. C*, 2010, **114**, 15499–15503.
29 S. B. Bashar, C. Wu, M. Suja, H. Tian, W. Shi and J. Liu, *Adv. Opt. Mater.*, 2016, **4**, 2063–2067.
30 X. Yang, L. Dong, C. Shan, J. Sun, N. Zhang, S. Wang, M. Jiang, B. Li, X. Xie and D. Shen, *Adv. Mater.*, 2017, **29**, 1602832.
31 G. Y. Zhu, J. T. Li, Z. S. Tian, J. Dai, Y. Y. Wang, P. L. Li and C. X. Xu, *Appl. Phys. Lett.*, 2015, **106**, 2230.

 This journal is © The Royal Society of Chemistry 2018

Published on 12 September 2018. Downloaded by Library of Chinese Academy of Sciences on 5/20/2019 6:59:12 AM.

32 J. Dai, C. Xu, T. Nakamura, Y. Wang, J. Li and Y. Lin, *Opt. Express*, 2014, **22**, 28831.
33 Q. Zhu, F. Qin, J. Lu, Z. Zhu, Z. Shi and C. Xu, *Opt. Mater.*, 2016, **60**, 366–372.
34 M. Jiang, G. He, H. Chen, Z. Zhang, L. Zheng, C. Shan, D. Shen and X. Fang, *Small*, 2017, **13**, 1604034.
35 L. Yang, M. Jiang, G. He, S. Li, Z. Zhang, B. Li, H. Zhao, C. Shan and D. Z. Shen, *ACS Appl. Mater. Interfaces*, 2017, **9**, 40743.
36 Y. Liu, M. Jiang, Z. Zhang, B. Li, H. Zhao, C. Shan and D. Shen, *Nanoscale*, 2018, **10**, 5678–5688.
37 M. Villafuerte, J. Ferreyra, C. Zapata, J. Barzola-Quiquia, F. Iikawa, P. Esquinazi, S. Heluani, M. de Lima Jr. and A. Cantarero, *J. Appl. Physiol.*, 2014, **115**, 133101.
38 G. D. Yuan, W. J. Zhang, J. S. Jie, X. Fan, J. X. Tang, I. Shafiq, Z. Z. Ye, C. S. Lee and S. T. Lee, *Adv. Mater.*, 2010, **20**, 168–173.
39 X. Zhang, L. Li, J. Su, Y. Wang, Y. Shi, X. Ren, N. Liu, A. Zhang, J. Zhou and Y. Gao, *Laser Photonics Rev.*, 2014, **8**, 429–435.
40 W. Ruane, K. Johansen, K. Leedy, D. C. Look, H. von Wenckstern, M. Grundmann, G. C. Farlow and L. J. Brillson, *Nanoscale*, 2016, **8**, 7631–7637.
41 G. H. He, M. M. Jiang, L. Dong, Z. Z. Zhang, B. H. Li, C. X. Shan and D. Z. Shen, *J. Mater. Chem. C*, 2017, **5**, 2542–2551.
42 Q. Wan, J. Huang, A. Lu and T. Wang, *Appl. Phys. Lett.*, 2008, **93**, 103109.
43 W. Liu, F. Xiu, K. Sun, Y.-H. Xie, K. L. Wang, Y. Wang, J. Zou, Z. Yang and J. Liu, *J. Am. Chem. Soc.*, 2010, **132**, 2498–2499.
44 X. Liu, Q. Zhang, J. N. Yip, Q. Xiong and T. C. Sum, *Nano Lett.*, 2013, **13**, 5336–5343.
45 J. Jeong, E. C. Ji, Y. J. Kim, S. Hwang, S. K. Kim, J. K. Kim, Y. J. Hu and Y. J. Hong, *Appl. Phys. Lett.*, 2016, **109**, 506.
46 C. F. Du, C. H. Lee, C. T. Cheng, K. H. Lin, J. K. Sheu and H. C. Hsu, *Nanoscale Res. Lett.*, 2014, **9**, 446.
47 Z. Zhang, Y. Wang, S. Yin, T. Hu, Y. Wang, L. Liao, S. Luo, J. Wang, X. Zhang and P. Ni, *Opt. Express*, 2017, **25**, 17375–17381.
48 A. Chen, H. Zhu, Y. Wu, G. Lou, Y. Liang, J. Li, Z. Chen, Y. Ren, X. Gui and S. P. Wang, *ACS Photonics*, 2017, **4**, 1286–1291.
49 G. Y. Zhu, C. X. Xu, Y. Lin, Z. L. Shi, J. T. Li, T. Ding, Z. S. Tian and G. F. Chen, *Appl. Phys. Lett.*, 2012, **101**, 041110.
50 X. Zhang, L. Li, J. Su, Y. Wang, Y. Shi, X. Ren, N. Liu, A. Zhang, J. Zhou and Y. Gao, *Laser Photonics Rev.*, 2014, **8**, 429–435.
51 L. Sun, Z. Chen, Q. Ren, K. Yu, L. Bai, W. Zhou, H. Xiong, Z. Q. Zhu and X. Shen, *Phys. Rev. Lett.*, 2008, **100**, 156403.
52 J. Lagois, *Phys. Rev. B: Condens. Matter Mater. Phys.*, 1981, **23**, 5511–5520.
53 L. Sun, H. Dong, W. Xie, Z. An, X. Shen and Z. Chen, *Opt. Express*, 2010, **18**, 15371–15376.
54 W. Du, S. Zhang, J. Shi, J. Chen, Z. Wu, Y. Mi, Z. Liu, Y. Li, X. Sui and T. Wu, *ACS Photonics*, 2018, **5**, 2051–2059.
55 D. Vanmaekelbergh and L. K. van Vugt, *Nanoscale*, 2011, **3**, 2783–2800.
56 X. Liu, Q. Zhang, Q. Xiong and T. C. Sum, *Nano Lett.*, 2013, **13**, 1080–1085.